The Spatial Alfvén Resonance
in a Collisional Plasma

I. J. Donnelly[A,B] *and B. E. Clancy*[A]

[A] Australian Atomic Energy Commission Research Establishment,
Private Mail Bag, Sutherland, N.S.W. 2232.
[B] Permanent address: School of Physics,
University of Sydney, Sydney, N.S.W. 2006.

Abstract

The structure of wave fields at the spatial Alfvén resonance in a cylindrical collisional plasma is studied using both a WKB analysis and a numerical solution of the wave equations. At high plasma density and low temperature the Alfvén resonance leads to ohmic dissipation of wave energy in a narrow resistive layer. The enhanced b_θ fields in this layer allow detection of the Alfvén resonance position by magnetic field probes. An experiment which reports the observation of the spatial Alfvén resonance has been analysed with good agreement between the calculated and the measured fields.

1. Introduction

The possibility of using the spatial Alfvén resonance for low frequency wave heating of plasmas was first proposed by Grossmann and Tataronis (1973) and by Hasegawa and Chen (1974). Appert *et al.* (1980) have calculated that significant damping of compressional wave eigenmodes is obtained in toroidal plasmas due to the Alfvén resonance, and they are proceeding with heating experiments. Ross *et al.* (1982) have given a kinetic theory description of Alfvén resonance heating in a hot plasma; their article contains a comprehensive summary of previous work.

Alfvén wave heating involves the excitation of a magnetohydrodynamic (MHD) wave, with given frequency and parallel wavenumber k, which 'sees' an infinite perpendicular refractive index at the Alfvén resonance surface where the condition $\omega^2 v_A^{-2}/(1 - \omega^2 \Omega_i^{-2}) = k^2$ is satisfied. Wave energy builds up around the resonance position until a balance between accumulation and dissipation is reached. Hasegawa and Chen (1976) and Kappraff and Tataronis (1977) have shown that the amount of energy lost by the MHD wave at the Alfvén resonance is, to a large extent, independent of the absorption mechanism. If the plasma is collisionless then mode conversion takes place and the energy propagates away in the form of an electrostatic wave. However, if the plasma is collisional then the energy is absorbed in a resistive layer around the resonance. Provided that the resistive layer is sufficiently narrow and enough energy is dissipated there, the wave fields near the resonance will be measurably larger than the global fields and the Alfvén resonance position can be detected by magnetic field probes. Such an experiment has been performed by Tsushima *et al.* (1982) in a cylindrical plasma using a Stix coil to excite MHD waves with well defined

wavenumbers m $(=0)$ and k. They found a reasonable correlation between the Alfvén resonance position and the peak of the $|b_\theta|$ field.

A series of experiments to investigate Alfvén wave heating and the behaviour of the wave fields near the Alfvén resonance is being conducted at the University of Sydney using the TORTUS tokamak (Cross *et al.* 1982). We are developing computer codes to calculate the antenna excitation of wave fields in a cylindrical model of the plasma. A kinetic theory plasma model is being developed but in the present paper a two-fluid theory is used. This is adequate for the analysis of low temperature plasmas, so we consider the behaviour of wave fields near the Alfvén resonance when the plasma is collisional and resistive damping is the primary dissipation mechanism.

In Section 2 the wave equations and the method of solution are described. Section 3 contains an approximate WKB analysis of the Alfvén resonance. This indicates the width of the resistive layer and the temperature limits for a collisional plasma. The experiment by Tsushima *et al.* (1982) is calculated in Section 4 and agreement is found between theory and experiment. Section 5 contains a range of numerical experiments which show the dependence of the Alfvén resonance fields on the plasma density and temperature and on the wave frequency. It is shown that the resistive layer could be observed in a high density low temperature tokamak discharge by using magnetic field probes.

2. Wave Equations

The behaviour of small amplitude waves, propagating in a cylindrical plasma column with a density $\rho_0(r)$ and a constant magnetic field $B_0\hat{z}$, is considered. The electric and magnetic field components (E and b) of the wave have the form

$$E(r, t) = E(r) \exp\{i(m\theta + kz - \omega t)\}. \qquad (1)$$

By using the electron and ion fluid equations and including the effects of electron inertia, electron–ion collisions and electron pressure, the standard procedure outlined by Stix (1962) results in the following wave equation, which is appropriate for a low temperature low β plasma and frequencies near or below the ion cyclotron frequency Ω_i:

$$\nabla \times \nabla \times E = \mathbf{u} . E, \qquad (2)$$

with

$$\mathbf{u} = \begin{pmatrix} u_1 & i u_2 & 0 \\ -i u_2 & u_1 & 0 \\ 0 & 0 & u_3 \end{pmatrix}.$$

Here

$$u_1 = \omega^2/\{v_A^2(1-f^2)\}, \qquad u_2 = u_1 f,$$

$$u_3 = -\frac{\omega^2 \Pi_i^2}{c^2(\omega^2 + i\omega\nu_{ei})} - \frac{\omega^2 \Pi_e^2}{c^2(\omega^2 - v_e^2 k^2 + i\omega\nu_{ei})},$$

where $f = \omega/\Omega_i$ and $v_e^2 = KT_e/m_e$. Also, v_A is the Alfvén speed, ν_{ei} is the electron–ion collision frequency and Π_α is the plasma frequency. The displacement current terms are small and have been omitted. Collisional terms have been omitted from the above

equations for u_1 and u_2, but they are included in the numerical calculations using the expressions given by Akhiezer *et al.* (1958). They are of minor importance as the collisional component in u_3 dominates the resistive damping at the spatial Alfvén resonance. The omission of ion temperature effects makes little difference to the results reported here.

Combining equation (2) with Maxwell's equation,

$$\nabla \times \boldsymbol{E} = -\partial \boldsymbol{b}/\partial t, \tag{3}$$

and eliminating the fields E_r and b_r results in the following set of four first-order coupled differential equations:

$$\frac{u_1}{r}\frac{\mathrm{d}rE_\theta}{\mathrm{d}r} = \frac{m}{r}u_2 E_\theta + \frac{m}{r}kp_\theta + \left(u_1 - \frac{m^2}{r^2}\right)p_z, \tag{4}$$

$$u_1\frac{\mathrm{d}E_z}{\mathrm{d}r} = ku_2 E_\theta - (u_1 - k^2)p_\theta - \frac{m}{r}kp_z, \tag{5}$$

$$\frac{1}{r}\frac{\mathrm{d}rp_\theta}{\mathrm{d}r} = \frac{m}{r}kE_\theta + \left(u_3 - \frac{m^2}{r^2}\right)E_z, \tag{6}$$

$$u_1\frac{\mathrm{d}p_z}{\mathrm{d}r} = \{u_2^2 - u_1(u_1 - k^2)\}E_\theta - \frac{m}{r}ku_1 E_z + ku_2 p_\theta - \frac{m}{r}u_2 p_z, \tag{7}$$

where

$$\boldsymbol{p} = -\partial \boldsymbol{b}/\partial t.$$

The plasma column, of radius a, is surrounded by a vacuum layer and a conducting wall at radius d. Plasma waves are excited by a divergence-free sheet current of the form

$$\boldsymbol{J}(r,t) = \mathbf{I}\,\delta(r-b)\frac{k\hat{\boldsymbol{\theta}} - mb^{-1}\hat{\boldsymbol{z}}}{\{k^2 + (mb^{-1})^2\}^{\frac{1}{2}}}\exp\{\mathrm{i}(m\theta + kz - \omega t)\}, \tag{8}$$

which is situated between the plasma and the wall.

In each of the plasma–antenna and antenna–wall vacuum regions, the wave fields can be expressed in terms of four independent solutions which are combinations of the modified Bessel functions $I_m(kr)$ and $K_m(kr)$ and their derivatives. In the plasma, equations (4)–(7) present a set of stiff differential equations which are solved as an initial value problem using Gears method (Hindmarsh 1974). The number of independent solutions in the plasma is reduced from four to two by the requirement that the fields are to be well behaved at the origin. The ten independent solutions are combined to satisfy the conditions that E_θ, E_z, b_θ and b_z are continuous at the plasma–vacuum boundary, that E_θ and E_z are continuous across the antenna where b_θ and b_z have known discontinuities proportional to $\boldsymbol{J}$, and that E_θ and E_z are zero at the wall. This combination is the required solution of the wave equations excited by the current source.

3. Approximate Analysis of the Spatial Alfvén Resonance

The procedure just described allows the calculation of wave fields excited in the plasma for any desired plasma parameters in the range of validity of the wave equation

(2). Of particular interest is the behaviour of the wave fields in the vicinity of the spatial Alfvén resonance and the dependence of these fields on plasma temperature and density, magnetic field strength and wave frequency. To provide some insight and guidance for the numerical work, a very simple treatment of the Alfvén resonance is developed in this section.

Consider first a constant density plasma. Following the method of Woods (1962), or by manipulation of equations (4)–(7) to obtain a fourth-order differential equation for $b_z(r)$, shows that two wave modes exist, with fields

$$b_r(r, k_c) = i\,Cm\frac{J_m(k_c r)}{k_c r} + i\,AK\frac{dJ_m(k_c r)}{d(k_c r)}, \tag{9a}$$

$$b_\theta(r, k_c) = -C\frac{dJ_m(k_c r)}{d(k_c r)} - Amk\frac{J_m(k_c r)}{k_c r}, \tag{9b}$$

$$b_z(r, k_c) = Ak_c J_m(k_c r), \tag{9c}$$

where J_m is a Bessel function of the first kind, k_c^2 is a root of

$$u_1 k_c^4 - \{(u_3 + u_1)(u_1 - k^2) - u_2^2\}k_c^2 + u_3\{(u_1 - k^2)^2 - u_2^2\} = 0, \tag{10}$$

and C and A are constants in the ratio

$$C/A = \{u_1(u_1 - k_c^2 - k^2) - u_2^2\}/u_2 k = \{\omega^2 v_A^{-2} - (k_c^2 + k^2)\}/fk. \tag{11}$$

In general $|u_3| \gg |u_1|$ and so, as long as the Alfvén resonance condition

$$u_1 - k^2 = 0 \tag{12}$$

is not approximately satisfied, the two solutions of (10) are

$$k_-^2 = \{(u_1 - k^2)^2 - u_2^2\}/(u_1 - k^2), \tag{13}$$

$$k_+^2 = u_3(u_1 - k^2)/u_1. \tag{14}$$

It is apparent under the above conditions that $|k_+| \gg |k_-|$. The wave associated with wavenumber k_- is henceforth called the MHD mode, and it is appropriate for the conditions considered here to term the wave with wavenumber k_+ the resistive mode.

When the Alfvén resonance condition (12) is satisfied the wavenumbers are of similar magnitude:

$$|k_-|^2 \approx |k_+|^2 \approx f|u_1 u_3|^{\frac{1}{2}}. \tag{15}$$

It is apparent from equations (9) that b_θ is the dominant field component for both the MHD and resistive modes in this case.

The wave behaviour near the Alfvén resonance is now considered for a plasma with a radial density variation. It is known from studies of Alfvén wave heating (see e.g. Hasegawa and Chen 1976) that the MHD wave propagates energy into the Alfvén resonance layer where it is mode converted into a short wavelength electrostatic wave which carries the energy away. The wave equations used here are sufficiently general

to show this behaviour, although a kinetic theory treatment is needed for a complete description in a collisionless plasma. Provided that v_{ei} is small, the electrostatic wave propagates towards regions of low plasma density if $\omega > v_e k$ but in the opposite direction if $\omega < v_e k$, as discussed by Stix (1980). In the former case it is termed a surface electrostatic wave, in the latter a kinetic Alfvén wave. For the purposes of this study a collisional plasma is defined as one in which the electrostatic wave (the resistive mode) is so heavily damped by electron–ion collisions that the energy lost by the MHD wave is deposited by ohmic heating in the immediate vicinity of the Alfvén resonance. The above condition is met if k_+ has a large imaginary component on both sides of the resonance, so equations (14) and (15) imply that u_3 is predominantly imaginary. The plasma is therefore classified as collisional if

$$\omega v_{ei} > \max(\omega^2, v_e^2 k^2)$$

at the Alfvén resonance position r_0. This condition can be expressed in the temperature form

$$T_e(r_0) < \min[16\{n_e(r_0) A/fB_0\}^{2/3}, 20\{(1-f^2)ZB_0/f\}^{2/5}], \qquad (16)$$

where T_e is in eV, Z and A are the ion charge and mass numbers, B_0 is in T and $n_e(r_0)$ is the electron number density in $10^{20}\,\mathrm{m}^{-3}$. It appears at first sight that a less stringent condition applies to v_{ei} when $\omega \approx v_e k$. However, Landau damping becomes important in this case and it dominates collisional effects if v_{ei} is too small. The strong Landau damping that occurs in a collisionless plasma when $\omega \approx v_e k$ probably leads to wave fields similar to those obtained here with collisional damping.

A lower limit on the temperature range of interest comes from the condition that $|u_3| \gg |u_1|$ (we assume $|u_3| > 10|u_1|$). Unless this is so $|k_-|$ and $|k_+|$ are of the same magnitude and there is little enhancement of the wave fields at the resonance layer. A fully ionized plasma is assumed here, and this imposes the additional condition $T_e(r_0) > 1$ eV. These two constraints give

$$T_e(r_0) > \max[0\cdot5\{fZn_e(r_0)/(1-f^2)B_0\}^{2/3}, 1]. \qquad (17)$$

The mode conversion process dumps energy into the resistive mode where it is rapidly dissipated. Provided that $|u_3| \gg |u_1|$, the width of the resistive layer is determined by the resistive mode wave fields. An estimate of this width is obtained by assuming a linear variation of the density at the Alfvén resonance and using the WKB approximation for k_+ to estimate the shape of the wave fields. Equations (9), (14) and (15) show that b_θ is the major field for the resistive mode. We assume that b_θ has its peak value at r_0. If the resistive layer is sufficiently narrow then in its vicinity the b_θ field has the approximate variation

$$b_\theta(r) = b_\theta(r_0)\exp\{i\,k_+(r-r_0)\}.$$

An estimate of the half-width of the b_θ field is given by

$$\Delta = r_2 - r_1,$$

where

$$\int_{r_1}^{r_0} |\operatorname{Im} k_+|\,\mathrm{d}r = \int_{r_0}^{r_2} |\operatorname{Im} k_+|\,\mathrm{d}r = \ln 0\cdot5.$$

If we assume an appreciable density gradient and a collisional plasma, equation (14) provides a reasonable approximation for k_+ in the above integrals, and

$$\Delta = 2 \cdot 6(c^2 v_{ei} l/\omega \Pi_e^2)^{1/3} = \{0 \cdot 07/T_e^{\frac{1}{4}}(r_0)\}(lA/fB_0)^{1/3} \text{ m}, \tag{18}$$

where

$$l = |\rho_0/(\mathrm{d}\rho_0/\mathrm{d}r)|_{r_0} \text{ m}.$$

This expression for Δ has the same dependence on plasma and wave parameters as that found by Kappraff and Tataronis (1977) using a boundary layer analysis of the incompressible MHD equations at low frequency; however, the coefficient is about $0 \cdot 1$ of their value. A rough guide to the scaling of the maximum value of $|b_\theta|$ in the resistive layer can be obtained using the fact that, for a collisional plasma with a well defined resistive layer, the energy dissipation in the resistive layer is almost independent of temperature. Therefore we have

$$\eta j_z^2 \Delta \propto \eta |b_\theta|_{\max}^2/\Delta = \text{a constant},$$

so that

$$|b_\theta|_{\max} \propto T_e^{\frac{1}{4}}(lA/fB_0)^{1/6}.$$

A condition for the resistive layer to be observable in a given plasma of radius a is $\Delta \ll a$. A further condition is that sufficient energy is to be deposited at the Alfvén resonance. A quantitative analysis of the energy deposition will be given elsewhere in connection with plasma heating. Other authors (see e.g. Karney *et al.* 1979) have also considered this problem and found that the energy deposition is given approximately by a term of the form $\gamma\omega(f+\varepsilon m)^2$, where γ and ε are functions of k and the plasma parameters. When $m = 0$, frequencies approaching Ω_i are needed to give enhanced fields at the spatial Alfvén resonance.

Table 1.   Temperature limits and the associated resistive layer widths

B_0 (T)	$n_e(r_0)$ (10^{20} m^{-3})	$T_{\min}$ (eV)	$\Delta(T_{\min})$ (cm)	$T_{\max}$ (eV)	$\Delta(T_{\max})$ (cm)
0·25	0·1	1·0	4·2	14	1·1
	1·0	1·0	4·2	14	1·1
	10·0	4·4	2·1	14	1·1
1·0	0·1	1·0	2·7	6	1·1
	1·0	1·0	2·7	24	0·5
	10·0	1·8	2·0	24	0·5
4·0	0·1	1	1·7	2	1·1
	1·0	1	1·7	10	0·5
	10·0	1	1·7	41	0·3

In Table 1 the upper and lower temperature limits from equations (16) and (17) are given for a range of B_0 and $n_e(r_0)$ in a hydrogen plasma at the normalized frequency $f = \frac{1}{2}$. The plasma density distribution used is

$$\rho_0(r) = \rho_0(1 - ra^{-1}); \qquad 0 \leqslant r \leqslant a,$$

so equation (18) gives

$$\Delta = \{0 \cdot 09/T_e^{\frac{1}{4}}(r_0)\}\{(a-r_0)/B_0\}^{1/3} \text{ m}.$$

It is apparent that Δ/a decreases as a increases. The tabulated values of Δ are given for $r_0 = \frac{1}{2}a$ and $a = 5\cdot5$ cm.

The analysis of this section indicates that enhanced b_θ fields at the spatial Alfvén resonance are most apparent when ω approaches Ω_i, B_0 is large and T_e is near the upper limit for a collisional plasma.

4. Comparison of Theory with Experiment

Tsushima *et al.* (1982) (henceforth referred to as TAI) have recently reported observations of the spatial Alfvén resonance excited by an axisymmetric ($m = 0$) Stix coil surrounding a cylindrical plasma. In this section we compare our calculations of the excited fields with their experimental results. A Fourier decomposition models the Stix coil by a sum of current sheets of the form given in equation (8). The wave fields excited by each current sheet are calculated and then summed to obtain the overall response.

TAI studied a singly ionized ^{4}He plasma with $T_e \approx T_i \approx 4$ eV, $n_{e0} \approx 5 \times 10^{20}$ m^{-3} and $B_0 = 0\cdot25$ T. We fit their density distribution by the function

$$n_e(r) = n_{e0}(1 - r^2 a^{-2})^{1.5}, \tag{19}$$

where $a = 5\cdot5$ cm, with agreement to within 10%. We also assume that $T_e(r)$ has a constant value of 4 eV.

The Stix coil is periodic in the z-direction with wavelength λ, so only the region $-\frac{1}{2}\lambda \leqslant z \leqslant \frac{1}{2}\lambda$ needs to be considered. We model the coil current by

$$\boldsymbol{J}(r, t) = \mathrm{I}\hat{\boldsymbol{\theta}}\,\delta(r - b)\,\{h(z - \tfrac{1}{2}\lambda) - h(z + \tfrac{1}{2}\lambda)\}\exp(-\mathrm{i}\,\omega t), \tag{20}$$

where

$$h(\xi) = 1/2w, \qquad -w \leqslant \xi \leqslant w;$$

$$= 0, \qquad \text{elsewhere},$$

and $w = 1$ cm. The coil radius b is $6\cdot5$ cm and there is a conducting boundary at $d = 7\cdot5$ cm. A Fourier transform of equation (20) gives

$$\boldsymbol{J}(r, t) = \frac{4\mathrm{I}}{\lambda}\hat{\boldsymbol{\theta}}\,\delta(r - b)\sum_{n=1,3}^{\infty}(-1)^{\frac{1}{2}(n-1)}\frac{\sin(k_n w)}{k_n w}\sin(k_n z)\exp(-\mathrm{i}\,\omega t), \tag{21}$$

where $k_n = 2\pi n/\lambda$. Replacing $\sin(k_n z)$ by $\{\exp(\mathrm{i}\,k_n z) - \exp(-\mathrm{i}\,k_n z)\}/2\mathrm{i}$ brings equation (21) to a sum of terms of the form given in equation (8). The overall wave fields are

$$F(r, t) = \frac{4\mathrm{I}}{\lambda}\sum_{n=1,3}^{\infty}(-1)^{\frac{1}{2}(n-1)}\frac{\sin(k_n w)}{k_n w}F_n(r)\sin(k_n z)\exp(-\mathrm{i}\,\omega t), \tag{22}$$

when $F = E_r$, E_θ or b_z, and

$$F(r, t) = -\frac{4\mathrm{i}\,\mathrm{I}}{\lambda}\sum_{n=1,3}^{\infty}(-1)^{\frac{1}{2}(n-1)}\frac{\sin(k_n w)}{k_n w}F_n(r)\cos(k_n z)\exp(-\mathrm{i}\,\omega t), \tag{23}$$

when $F = E_z$, b_r or b_θ. The fields $F_n(r)$ are obtained by solving equations (4)–(7) with the sheet current

$$\boldsymbol{J}_n(r, t) = \hat{\boldsymbol{\theta}}\,\delta(r - b)\exp\{\mathrm{i}(k_n z - \omega t)\}.$$
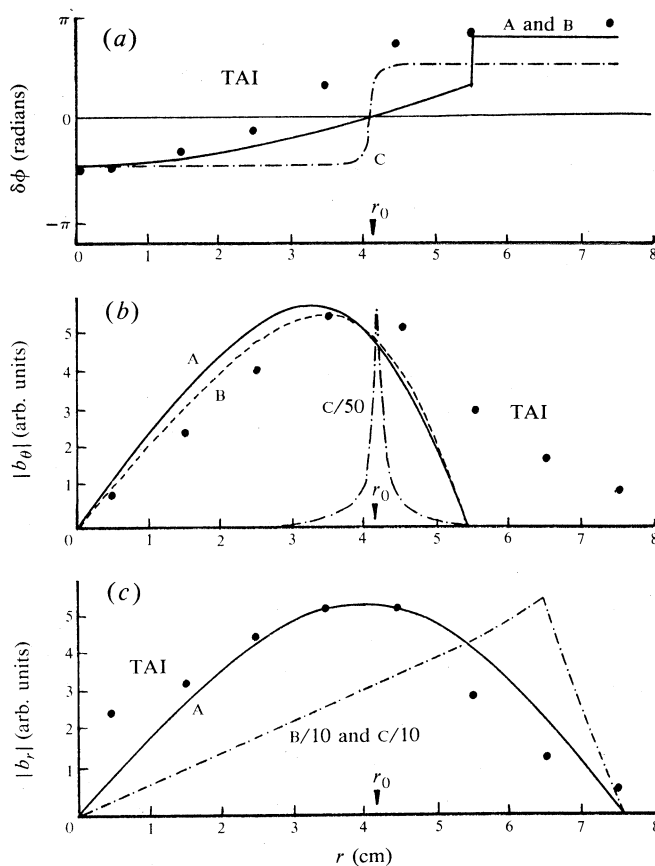
Fig. 1. Comparison of calculated field profiles at $z = 0$ with the measured fields reported by TAI at 480 kHz. Curve A is the converged 30 mode solution, curve B the $n = 1$ mode only and curve C the $n = 1$ mode solution of the MHD equations.
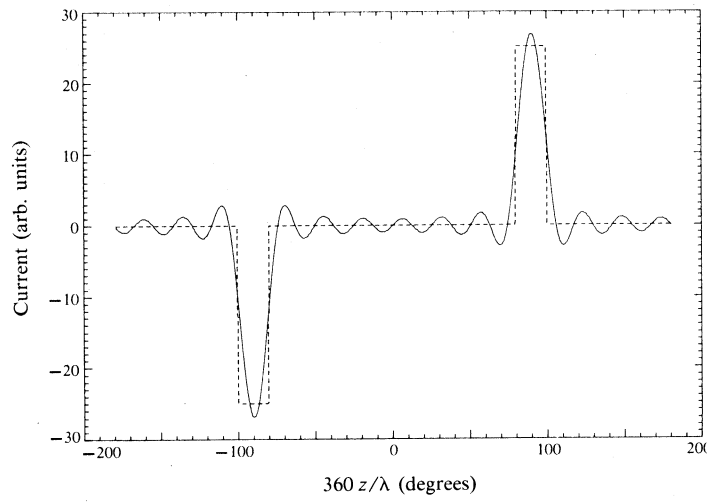

Fig. 2. Seven mode Fourier representation of the Stix coil current distribution.

We define the phase angles ϕ by

$$b_r = |b_r| \exp(\mathrm{i}\,\phi_r), \qquad b_\theta = |b_\theta| \exp(\mathrm{i}\,\phi_\theta), \qquad \delta\phi = \phi_r - \phi_\theta.$$

The radial profiles of $|b_r|$, $|b_\theta|$ and $\delta\phi$ at $z = 0$ are compared in Fig. 1 with the values measured by TAI at a frequency of 480 kHz with $\lambda = 40$ cm. Three sets of calculated fields are shown. In curve A the first 30 modes ($n = 1$–59) are included in equations (22) and (23); curve B consists of the $n = 1$ mode only; and curve C is the $n = 1$ mode solution of the MHD equations with the Hall term. For each curve A, $|b_r|$ and $|b_\theta|$ are normalized to the same maximum values as the measured fields, and the same normalization factor is applied to the B and C fields. In the vacuum region b_θ is zero so we set $\phi_\theta(r \geqslant a) = \phi_\theta(r = a^-)$. There is reasonable agreement between the A fields and the measured fields, with the major discrepancy occurring in $|b_\theta|$ and $\delta\phi$ near the plasma edge. The extension of the measured b_θ field beyond the plasma edge is probably due to the presence of neutrals which couple to any plasma present and enhance the effective plasma density by the factor

$$S = 1 + \rho_{0\mathrm{n}}\rho_0^{-1}/(1 - \mathrm{i}\,\omega v_{\mathrm{ni}}^{-1}),$$

where v_{ni} is the neutral–ion collision frequency (Woods 1963).

A comparison of curves A and B indicates that $|b_\theta|$ converges quickly with N, the maximum n value included in equation (23), and it is given predominantly by the $n = 1$ mode. This is not unexpected since only the $n = 1$ mode excites the Alfvén resonance in the plasma for the given parameters and it therefore gives the major contribution to b_θ. Also, for n large, $b_{\theta,n}$ converges at a faster rate than n^{-2}. The single and 30 mode values of b_r are quite dissimilar, as can be seen in Fig. 1c where the field B is about ten times as large as A. The $b_{r,n}$ and $b_{z,n}$ fields become concentrated around the antenna radius as n increases. However, as their amplitudes are virtually independent of n, b_r and b_z converge only slowly, especially in the region near $r = b$. The rate of convergence is determined by the factor $(-1)^{\frac{1}{2}(n-1)}\sin(k_n w)/k_n w$. We have found that 10 modes are sufficient to converge b_r and b_z for $r < a$, but even the 30 mode solution contains appreciable spurious oscillations of b_r and b_z in the z-direction when $r \approx b$. They are related to the oscillations in the truncated Fourier series representation of the current distribution J_N, which is shown for $N = 13$ in Fig. 2. By evaluating b_r at those z values where $\mathrm{d}J_N/\mathrm{d}z = 0$, and b_z where $J_N(z) = 0$, these oscillations can effectively be averaged out and accurate fields obtained without considering an extremely large number of modes. The phase $\phi_{r,n}$ is approximately $-\pi$ for all n in this particular case so, since $b_\theta \approx b_{\theta,1}$, $\delta\phi$ is almost independent of N, thereby explaining the good agreement between the $\delta\phi$ curves A and B in Fig. 1a.

As b_θ is dominated by the $n = 1$ mode, then $b_\theta(r, z) \approx b_{\theta,1}(r)\cos(k_1 z)$. The higher order modes slightly shift the peak in $|b_\theta(r)|$ towards higher radius as $|z|$ goes from 0 to $\frac{1}{4}\lambda$. The peak in $|b_r(r, z)|$ moves towards the antenna radius and $b_r(r, z)$ increases in magnitude as $|z|$ goes from 0 to $\frac{1}{4}\lambda - w$. In the vicinity of the coil ($|z| \approx \frac{1}{4}\lambda$), b_r and b_z are essentially the vacuum induction fields of the antenna.

Curves C in Fig. 1 are calculated using the MHD equations with the Hall term and perpendicular resistivity but without electron inertia and parallel resistivity (so $E_z = 0$ and the resistive mode is omitted). It is apparent that the MHD equations are inadequate for the determination of b_θ near the Alfvén resonance.

Table 2.   Variation of the Alfvén resonance fields with frequency

The plasma parameters correspond to the experiment of Tsushima *et al.* (1982) with $\lambda = 40$ cm

ω/Ω_i	r_0 (cm)	r_θ (cm)	r_ϕ (cm)	Δ_θ (cm)	Δ (cm)	ω/Ω_i	r_0 (cm)	r_θ (cm)	r_ϕ (cm)	Δ_θ (cm)	Δ (cm)
0·304	0	2·65	Note[A]	3·44	—	0·417	3·48	2·95	3·20	3·63	3·06
0·306	0·37	2·68	Note[A]	3·44	8·48	0·504	4·18	3·43	4·35	3·56	2·40
0·317	1·35	2·70	Note[A]	3·44	5·33	0·584	4·57	3·78	5·03	3·31	2·00
0·334	2·02	2·70	Note[A]	3·50	4·46	0·751	5·09	4·12	5·45	3·09	1·37
0·384	3·05	2·84	2·25	3·59	3·45	0·912	5·43	4·15	5·50	3·19	0·71

[A] $\delta\phi$ has no zero.

Table 2 shows the variation with frequency of several parameters which describe the Alfvén resonance. The terms r_θ, r_ϕ and Δ_θ are defined as follows: r_θ is the radius at which $|b_\theta|$ is a maximum, r_ϕ is the radius at which $\delta\phi = 0$ and Δ_θ is the width of $|b_\theta|$ at half maximum. The half-width Δ is obtained from equation (18). TAI have shown that a WKB analysis using the MHD wave equations indicates that $\delta\phi = 0$ at r_0 and it is of interest to see if a more complete analysis also shows this correlation. The predicted variation in r_θ with frequency agrees fairly well with the experimental results of TAI which show r_θ increasing from 2·5 cm, when $f = 0·3$, to 4·4 cm when $f = 0·7$. In Table 2, there is reasonable agreement between r_θ and r_0 for $2 \lesssim r_0 \lesssim 4$ cm. There is also reasonable agreement between r_ϕ and r_0 when $r_0 > 3$ cm, but $\delta\phi$ has no zero when $r_0 < 2·5$ cm. We note in passing that the MHD solution has almost perfect agreement between r_0, r_θ and r_ϕ over the frequency range for which the Alfvén resonance is present in the plasma. The half-width Δ_θ is virtually independent of frequency, in contrast to the behaviour predicted for Δ. For $r_0 < 1·3$ cm, the resistive layer is spread across the plasma because $\Delta > a$. When $r_0 \to a$ there are two possible reasons for the discrepancy between Δ and Δ_θ: firstly it can be seen from equation (16) that the second upper limit on T_e is being approached so there may be some broadening of the resistive layer by the kinetic Alfvén wave, and secondly equation (18) always underestimates the value of Δ_θ near the plasma edge if $\rho_0(a) = 0$.

In the next section we see that an increase in T_e, B_0 and ω leads to thinner resistive layers and better agreement between r_θ, r_ϕ and r_0 and also between Δ and Δ_θ.

5. Quantitative Analysis of the Alfvén Resonance

In this section the wave equations are solved for a range of densities, temperatures and frequencies, and the fields near the Alfvén resonance are examined in detail. A hydrogen plasma is considered with the density distribution defined in equation (19) and a constant temperature profile. A magnetic field of 1 T is used to obtain reasonably narrow resistive layers. Only single modes ($n = 1$), excited by the sheet current (8), are considered and, unless otherwise specified, $m = 0$.

At the low end of the density range appropriate for tokamaks, condition (16) indicates that the maximum temperature of a collisional plasma is fairly low. This is illustrated in Fig. 3 where profiles of $|b_\theta|$ are shown for $T_e = 1$, 3 and 5 eV, $n_{e0} = 2 \times 10^{19}$ m^{-3}, $f = 0·5$ and with $k = 8$ m^{-1} so that $n_e(r_0) = 0·5 n_{e0}$. When field profiles are compared in the following figures they have been excited by the same sheet current unless otherwise specified. The resistive layer is diffuse when $T_e = 1$ eV and then becomes

more peaked at 3 eV, but begins to broaden at 5 eV due to propagation of the surface electrostatic wave. The positions r_θ and r_ϕ, along with the half-widths Δ_θ and Δ (from equation 18), are compared in Table 3. The correlation of r_θ and r_ϕ with r_0 is good except that the appearance of the surface electrostatic wave leads to an extra zero for $\delta\phi$ when $T_e = 5$ eV. Equation (18) underestimates the resistive layer width by about a factor of 2 in this case.

Fig. 3. Comparison of $|b_\theta|$ fields for $T_e = 1$, 3 and 5 eV, $n_{eo} = 2 \times 10^{19}$ m^{-3}, $B_0 = 1$ T, $f = 0 \cdot 5$ and $k = 8$ m^{-1}. The surface electrostatic wave broadens the profile at 5 eV.

Table 3.   Variation of Alfvén resonance fields with temperature
The plasma and wave parameters are $n_{eo} = 2 \times 10^{19}$ m^{-3}, $B_0 = 1$ T, $f = 0 \cdot 5$
and $k = 8$ m^{-1}

T_e (eV)	r_0 (cm)	r_θ (cm)	r_ϕ (cm)	Δ_θ (cm)	Δ (cm)
1	3·43	3·00	3·41	3·5	2·3
3	3·43	3·40	3·60	2·4	1·3
5	3·43	3·45	3·75, 4·95	2·2	1·0

We consider now a high density plasma with $n_{eo} = 2 \times 10^{21}$ m^{-3}, which allows a larger range of temperatures. Profiles of $|b_\theta|$ are shown in Fig. 4 for $T_e = 1$, 5 and 20 eV, with $f = 0 \cdot 5$ and $k = 80$ m^{-1} so that $n_e(r_0) = 0 \cdot 5 n_{eo}$. The peaking of $|b_\theta|$ around r_0 as T_e increases is clear. There is some kinetic Alfvén wave propagation at 20 eV; it is still only marginal at 30 eV, with two zeros of $\delta\phi$ appearing in the range $r < r_0$, but at 50 eV it is strong with five zeros of $\delta\phi$. For $1 < T_e < 20$ eV the agreement between r_0, r_θ and r_ϕ is excellent, and $\Delta \approx 0 \cdot 6 \Delta_\theta$. The variation with frequency of Alfvén resonance fields at $T_e = 10$ eV is shown in Table 4. As r_0 moves from the plasma centre to the edge there is good agreement between r_0, r_θ and r_ϕ in the range $1 \lesssim r_0 \lesssim 5$ cm. Over most of this range $\Delta \approx 0 \cdot 6 \Delta_\theta$.

The frequency $f = 0 \cdot 79$ is of especial interest as it is the lowest eigenfrequency of the $m = 0$ compressional wave. The $|b_\theta|$ fields and the resistive energy deposition per unit volume are shown in Fig. 5 for $f = 0 \cdot 72$, $0 \cdot 79$ and $0 \cdot 89$. Under eigenmode conditions the global $|b_\theta|$ dominates the Alfvén resonance $|b_\theta|$. This dominance

decreases slightly with increasing temperature. Another point of interest is the virtual disappearance of spatial Alfvén resonance effects when $f = 0.80$, just above the eigenmode frequency. This phenomenon is also predicted by a simple model of Alfvén resonance heating; it will be discussed in detail elsewhere.
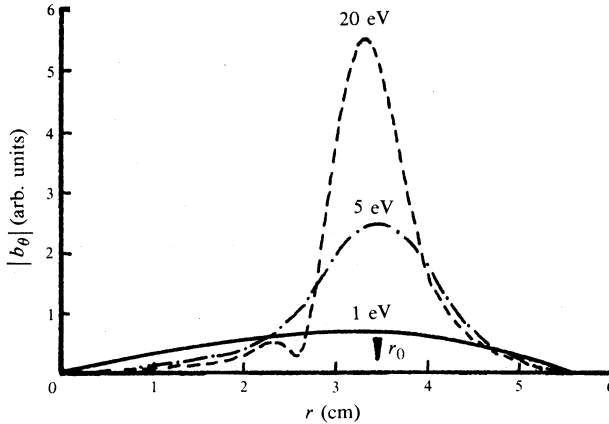

Fig. 4. Comparison of $|b_\theta|$ fields for $T_e = 1$, 5 and 20 eV, $n_{eo} = 2 \times 10^{21}$ m^{-3}, $B_0 = 1$ T, $f = 0.5$ and $k = 80$ m^{-1}. The kinetic Alfvén wave is just evident at 20 eV.

Table 4. Variation of Alfvén resonance fields with frequency

The plasma and wave parameters are $n_{eo} = 2 \times 10^{21}$ m^{-3}, $T_e = 10$ eV, $B_0 = 1$ T and $k = 80$ m^{-1}

ω/Ω_i	r_0 (cm)	r_θ (cm)	r_ϕ (cm)	Δ_θ (cm)	Δ (cm)	ω/Ω_i	r_0 (cm)	r_θ (cm)	r_ϕ (cm)	Δ_θ (cm)	Δ (cm)
0.38	0	1.10	Note^A	1.88	—	0.72	4.75	4.68	4.72	0.74	0.43
0.39	1.05	1.15	Note^A	1.88	1.37	0.78	4.93	4.85	4.93	0.72	0.38
0.42	2.17	2.20	2.05	1.69	1.01	0.79	4.97	4.80	4.97	Note^B	0.37
0.46	2.95	2.92	2.88	1.39	0.83	0.81	5.05	4.97	5.05	0.56	0.35
0.54	3.81	3.77	3.80	1.07	0.65	0.89	5.25	5.18	5.25	0.48	0.28
0.63	4.33	4.28	4.31	0.93	0.54						

^{A} $\delta\phi$ has no zero.

^{B} This is the lowest resonance frequency of the $m = 0$ compressional wave; Δ_θ cannot be measured in this case—see Fig. 5.

Finally the $\delta\phi$ and $|b_\theta|$ fields excited by current sheets with $m = -1$, 0 and 1 are compared in Fig. 6 for $n_{eo} = 2 \times 10^{21}$ m^{-3}, $T_e = 10$ eV, $B_0 = 1$ T, $f = 0.42$ and $k = 80$ m^{-1}. The $|b_\theta|$ curves have been normalized to the same peak value; for a given sheet current amplitude they are approximately in the ratio

$$|b_\theta(-1)| : |b_\theta(0)| : |b_\theta(1)| = 3 : 2 : 1,$$

but this ratio depends strongly on frequency and plasma parameters. The variation of r_θ with frequency is similar for all three m modes except near eigenfrequencies. The $m = -1$ mode normally has a zero in $\delta\phi$ near the origin as well as near r_0, and when r_0 is small these zeros can vanish. Similar behaviour is observed when $m = 1$ except that the extra zero is near the plasma edge and both zeros may disappear when r_0 nears the edge. Care must therefore be taken if the zero of $\delta\phi$ is used to identify r_0 in association with $m \neq 0$ waves.
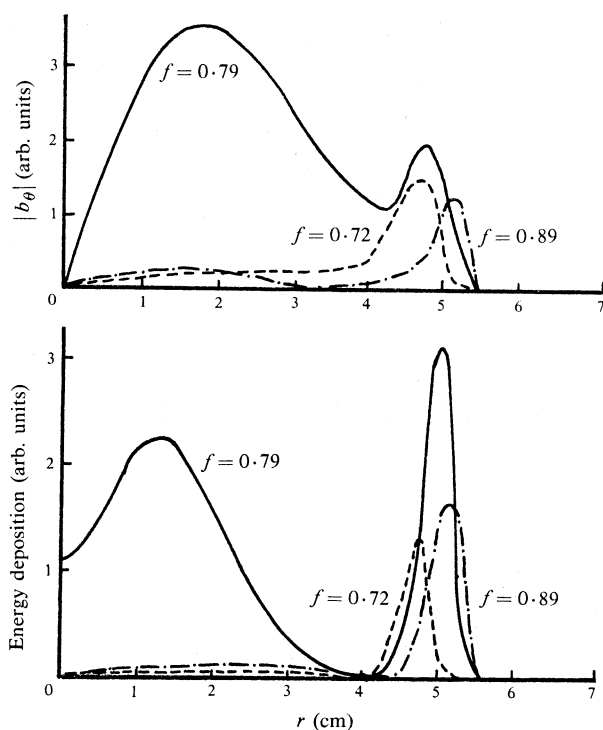
Fig. 5. Comparison of $|b_\theta|$ fields and the energy deposition per unit volume for $f = 0.72$, 0.79 and 0.89, $B_0 = 1$ T, $k = 80$ m^{-1}, $n_{eo} = 2 \times 10^{21}$ m^{-3} and $T_e = 10$ eV. The global $|b_\theta|$ and energy deposition are clearly enhanced at the eigenmode frequency $f = 0.79$.
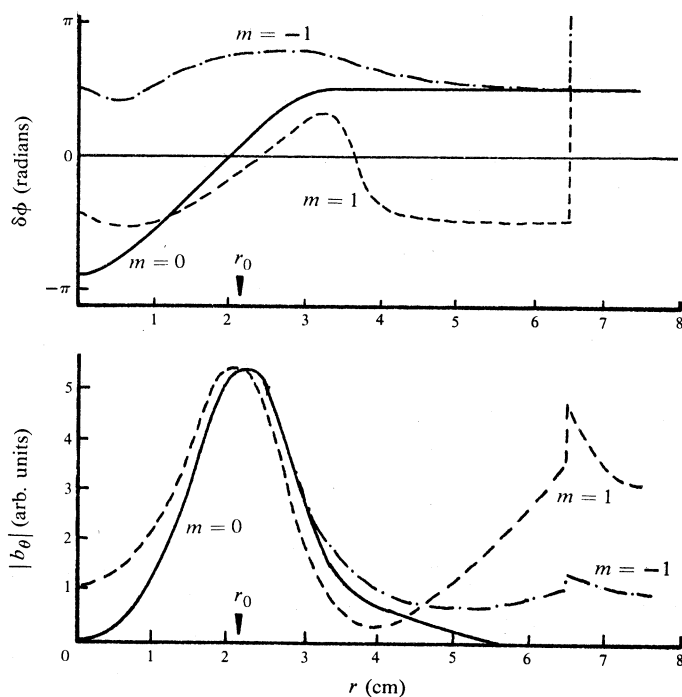

Fig. 6. Comparison of $\delta\phi$ and $|b_\theta|$ fields for $m = -1, 0, 1$, $n_{eo} = 2 \times 10^{21}$ m^{-3}, $T_e = 10$ eV, $B_0 = 1$ T, $f = 0.42$ and $k = 80$ m^{-1}. The $|b_\theta|$ fields are normalized to the same peak value. At this frequency the $m = -1$ mode has no zero for $\delta\phi$ and the $m = 1$ mode has two zeros.

6. Discussion

The spatial Alfvén resonance is of interest because it provides a mechanism for plasma heating. In a high temperature plasma, laser scattering off electrostatic wave density perturbations excited by mode conversion is probably the only means of probing the wave fields near the Alfvén resonance. However, in a low temperature plasma, magnetic field probes can be used as a diagnostic tool to measure the position, width and height of the resistive layer and thus enable a comparison between theory and experiment. It is apparent from equation (16) that the temperature at which mode conversion to electrostatic waves becomes important can be fairly low, and an interesting experiment would be the observation of a change from resistive dissipation to an excitation of electrostatic waves as, for example, T_e increased.

We have shown here that, with an appropriate choice of plasma and wave parameters, the resistive layer becomes narrow and the peak of $|b_\theta|$ lies very close to the Alfvén resonance position r_0. The position where $\delta\phi = 0$ also provides a good indication of r_0. These indicators break down, however, in the limits of high or low temperature. At high temperature the electrostatic wave begins to propagate, which broadens the resistive layer and leads to extra zeros in $\delta\phi$. At low temperatures the resistive layer becomes as wide as the plasma and the position of maximum $|b_\theta|$ varies little with r_0.

Care must also be exercised when using the zero of $\delta\phi$ as an indicator of r_0 in association with $m \neq 0$ waves. In the cases examined here both $m = 1$ and -1 waves have an extra zero at some frequencies and no zeros at others.

Finally, we point out that the simple analysis in Section 3 gives quite accurate temperature limits for the collisional regime. Also, providing the plasma is collisional and the resistive layer is narrow compared with the plasma radius, a good approximation for the half-width of $|b_\theta|$ is

$$\Delta_\theta = 1 \cdot 7 \, \Delta \,,$$

where Δ is given by equation (18).

References

Akhiezer, A. I., *et al.* (1958). Proc. 2nd U.N. Int. Conf. on Peaceful Uses of Atomic Energy, Geneva, Vol. 31, p. 99 (United Nations: Geneva).

Appert, K., Balet, B., Gruber, R., Troyon, F., Tsunematsu, T., and Vaclavik, J. (1980). Proc. 2nd Varenna–Grenoble Int. Symp. on Heating in Toroidal Plasmas, Como, Italy, p. 643 (Euratom: Brussels).

Cross, R. C., Blackwell, B. D., Brennan, M. H., Borg, G., and Lehane, J. A. (1982). Proc. 3rd Varenna–Grenoble Int. Symp. on Heating in Toroidal Plasmas, Grenoble, France, p. 177 (Euratom: Brussels).

Grossmann, W., and Tataronis, J. (1973). *Z. Phys.* **261**, 217.

Hasegawa, A., and Chen, L. (1974). *Phys. Rev. Lett.* **32**, 454.

Hasegawa, A., and Chen, L. (1976). *Phys. Fluids* **19**, 1924.

Hindmarsh, A. C. (1974). GEAR Ordinary Differential Equation Solver, Lawrence Livermore Lab. Rep. No. UCID-30001, Rev. 3.

Kappraff, J. M., and Tataronis, J. A. (1977). *J. Plasma Phys.* **18**, 209.
Karney, C. F. F., Perkins, F. W., and Sun, Y.-C. (1979). *Phys. Rev. Lett.* **42**, 1621.
Ross, D. W., Chen, G. L., and Mahajan, S. M., (1982). *Phys. Fluids* **25**, 652.
Stix, T. H. (1962). 'The Theory of Plasma Waves' (McGraw–Hill: New York).
Stix, T. H. (1980). Proc. 2nd Varenna–Grenoble Int. Symp. on Heating in Toroidal Plasmas, Como, Italy, p. 631 (Euratom: Brussels).
Tsushima, A., Amagishi, Y., and Inutake, M. (1982). *Phys. Lett.* A **88**, 457.
Woods, L. C. (1962). *J. Fluid Mech.* **13**, 570.
Woods, L. C. (1963). *Phys. Fluids* **6**, 729.